THE AIR FORCE RESEARCH LABORATORY
LEAD | DISCOVER | DEVELOP | DELIVER

Nonlinear Plasma Effects in Natural and Man-made Aurora

Evgeny Mishin and Todd Pedersen

Space Vehicles Directorate

Air Force Research Laboratory

Bedford, MA, USA

Modern Challenges in Nonlinear Plasma Physics

15-19 June, 2009, Sani Resort, Halkidiki, Greece

OUTLINE

Natural and Artificial Auroras

- Introduction: "*Ordinary" and Enhanced Aurora*
- Collisional vs. Collisionless (Beam-Plasma) Interaction
- SLT Aurora: *Plasma Turbulence Layer*

❖Underlined text indicates **Dennis's significant contributions** to understanding these problems

HF-induced Airglow

- ✓ HF Modification Experiments at HAARP
- ✓ Parametric instabilities
- ✓ Electron acceleration

Optical Emissions

- Emissions stimulated by impact of energetic electrons on ambient species (N_2, O, O_2)
- Excitation energy an indicator of electron energy spectrum

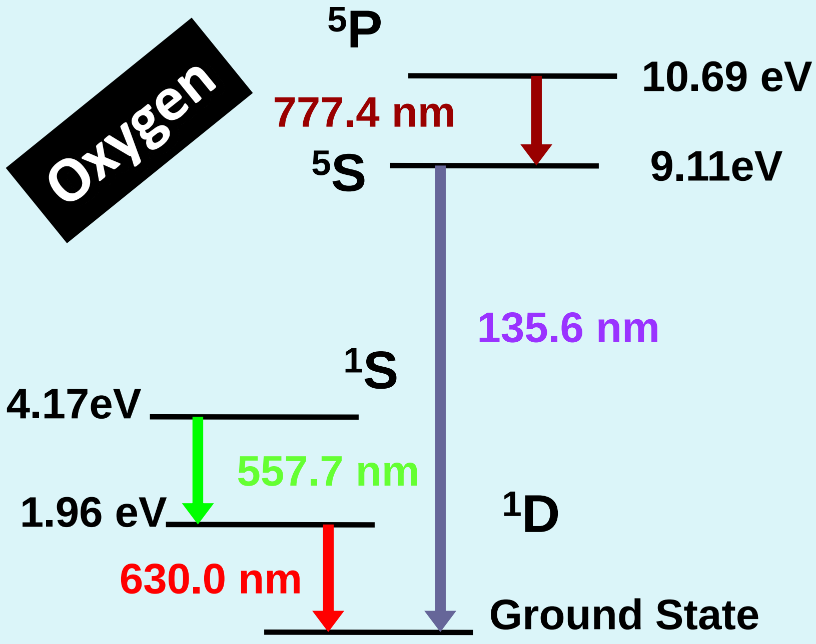

Green:	O(1S)	557.7 nm	~5 eV
Blue:	N2(2PG)	~400.0 nm;	11 eV
	N2+(1NG)	427.8 nm;	20 eV
Red:	N2(1PG)	676.5 nm;	7.4 eV
	O(1D)	630.0 nm;	~2 eV

Ordinary (*collisional*) Aurora

Precipitating (*primary*) electrons excite & ionize neutral particles via collisions

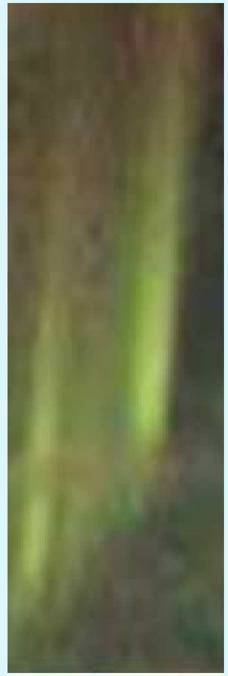

Energy dissipation rate

(Bethe's formula)

$$d\varepsilon_b / dz \cong -\varepsilon_b / l_b$$

$$l_{b\,[\mathrm{km}]} \simeq 5 \frac{N_{[120km]}}{N} \sqrt{\varepsilon_{b\,[\mathrm{keV}]}}$$

Flux of suprathermal (secondary) electrons

defines brightness and colors of auroral glow

$$\Phi(\varepsilon) \propto \varepsilon^{-3.5}$$

~6 to ~300 eV

Auroral Ray Altitude Profile

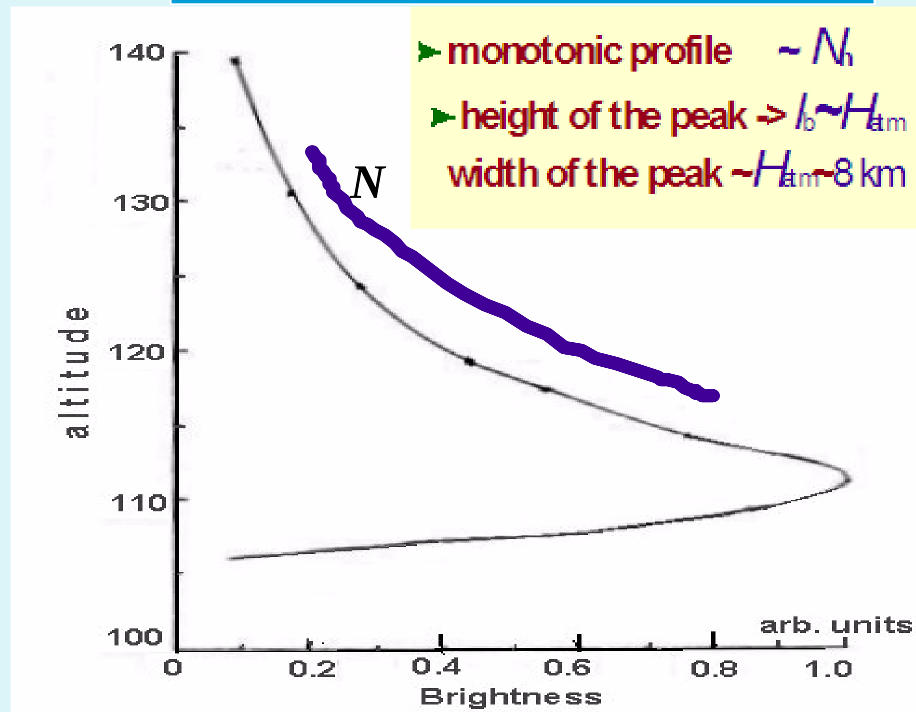

$$Q_\lambda = N_j \int \sigma_\lambda(\varepsilon)\Phi(\varepsilon,\vartheta)\,d\Omega\,d\varepsilon$$

neutral density

excitation cross-section

electron flux

Excitation rate

"Enhanced" Aurora

Sharp -gradient or double-peaked profiles

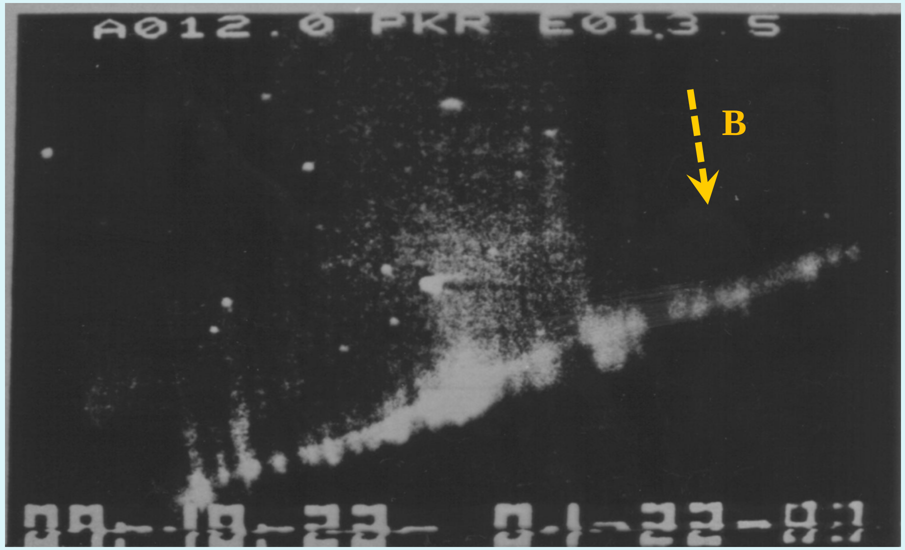

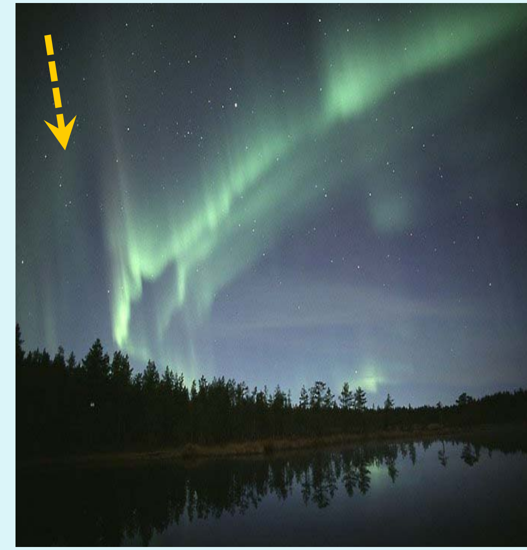

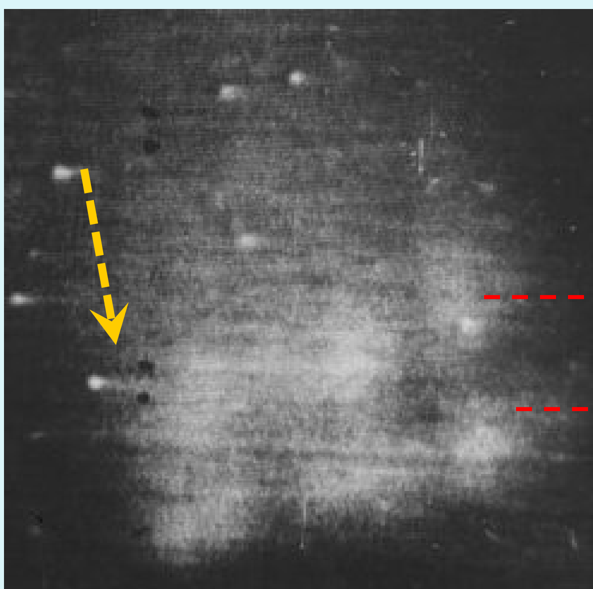

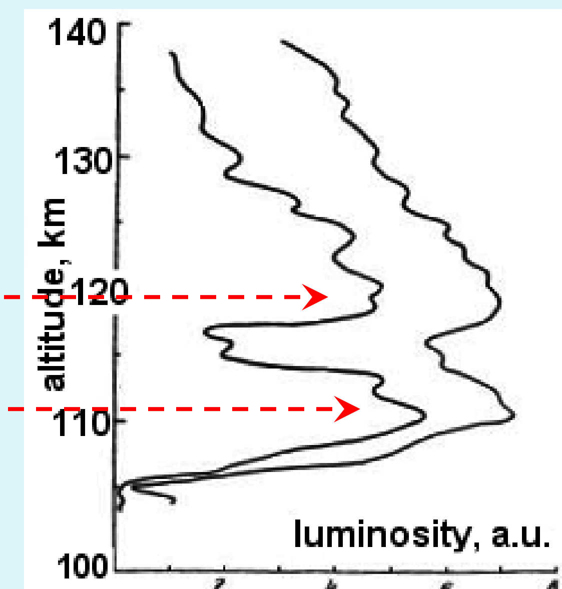

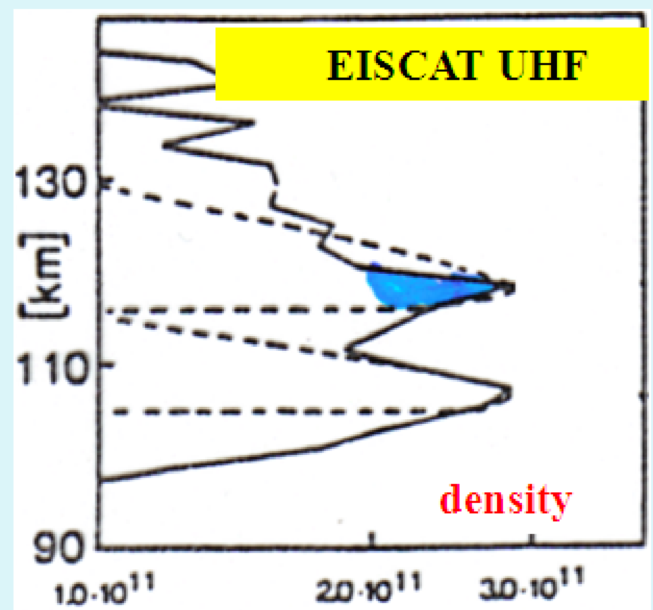

AA (active) Experiments

Zarnitsa-2 experiment (1975)

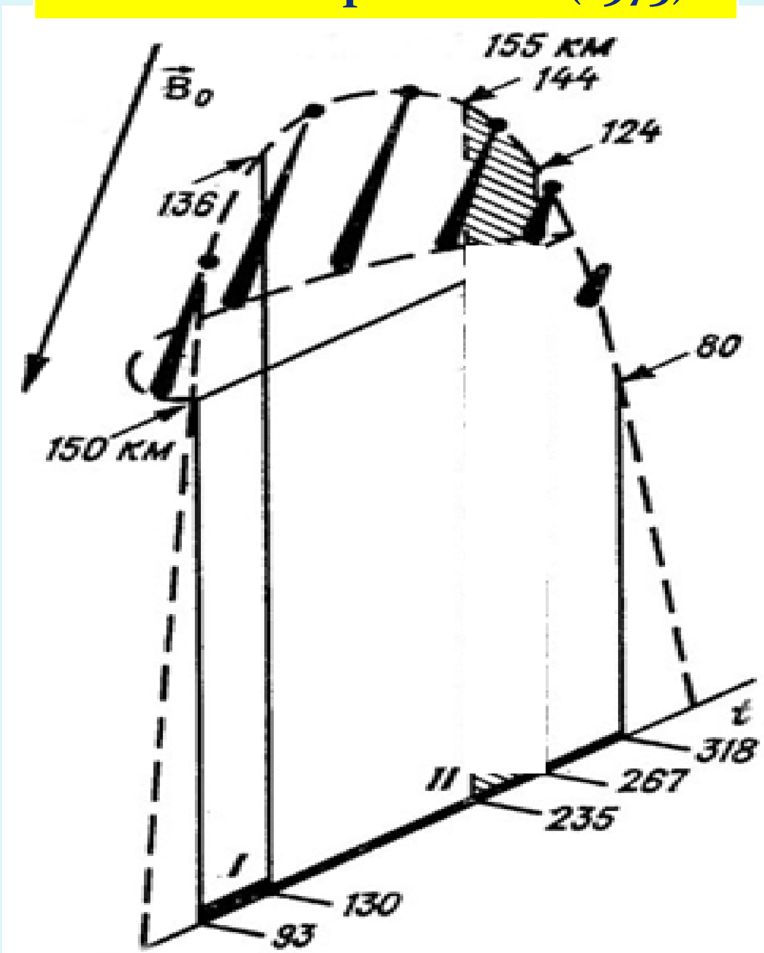

Low-light TV Observations

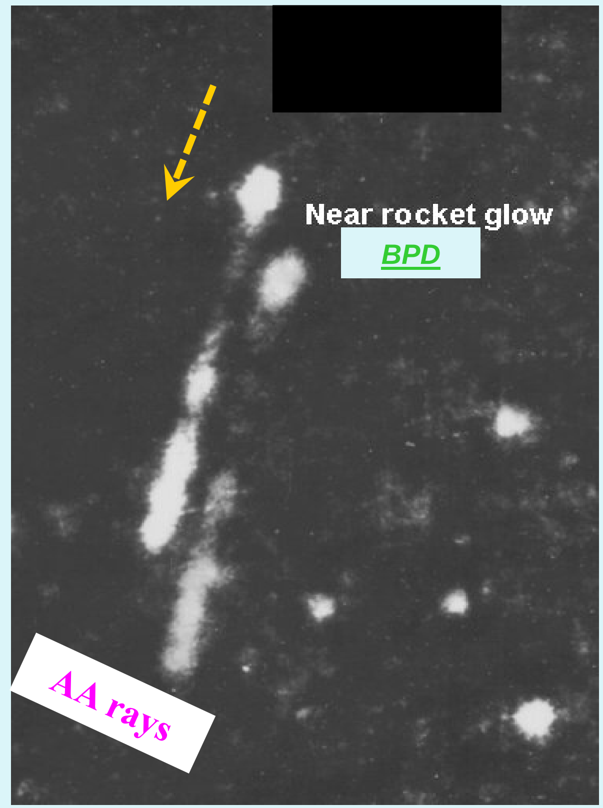

Artificial Aurora Rays

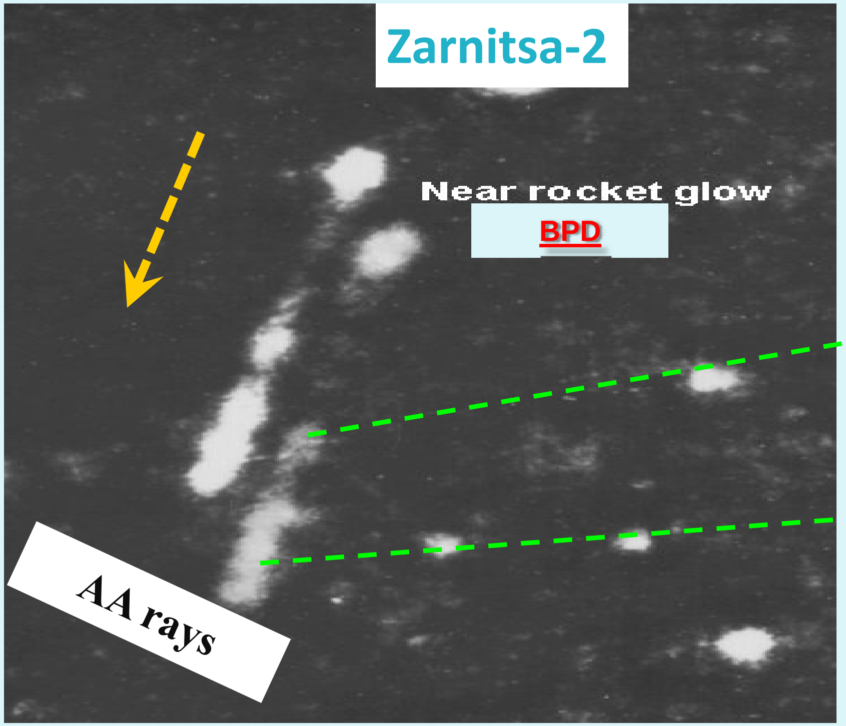

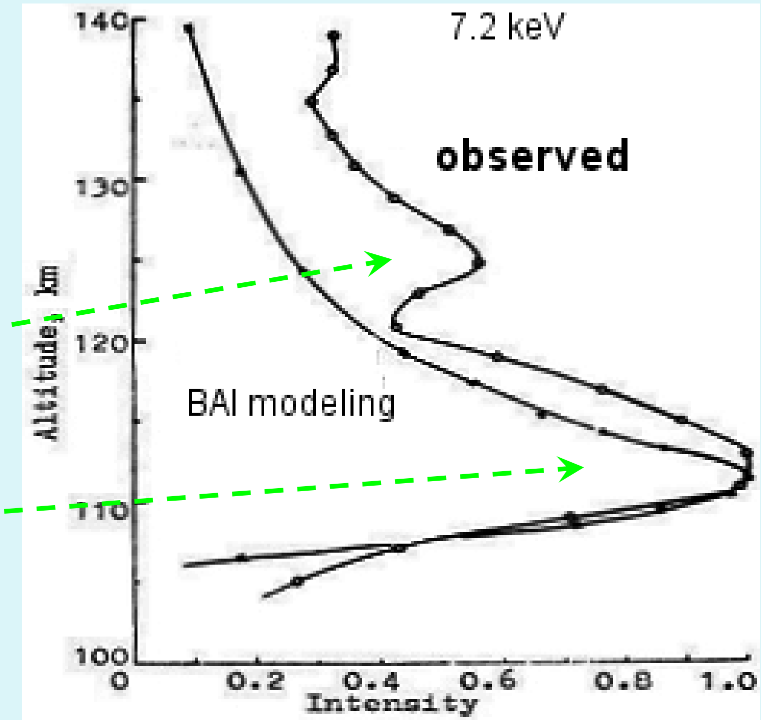

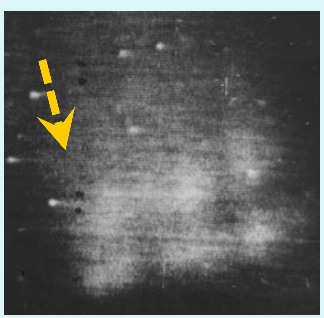

Enhanced Aurora

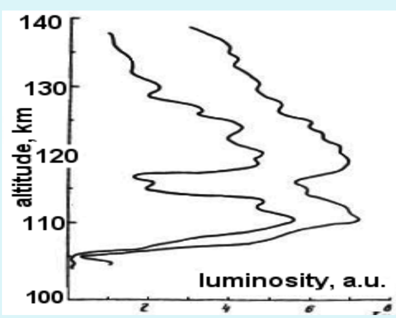

Mishin et al., 1981

Suprathermal Electrons

Natural Auroras

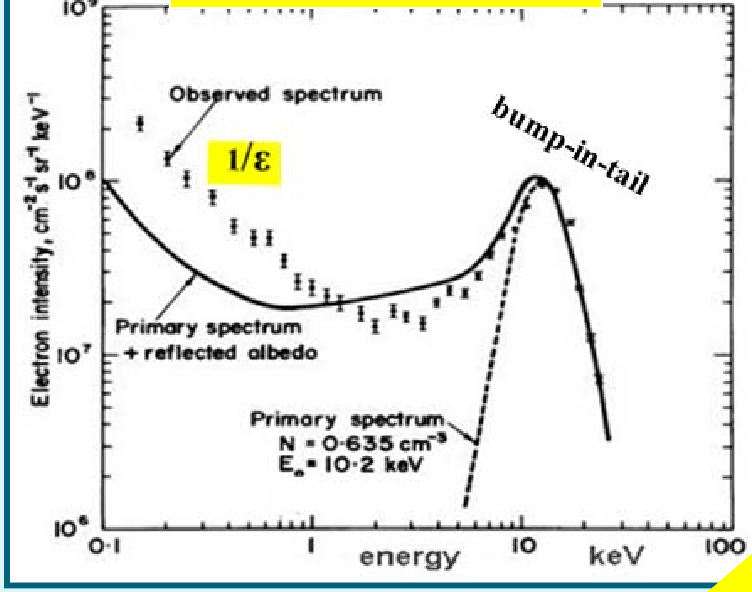

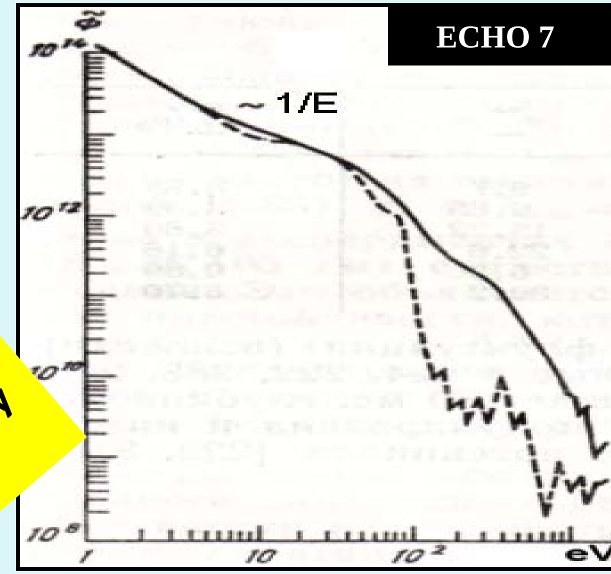

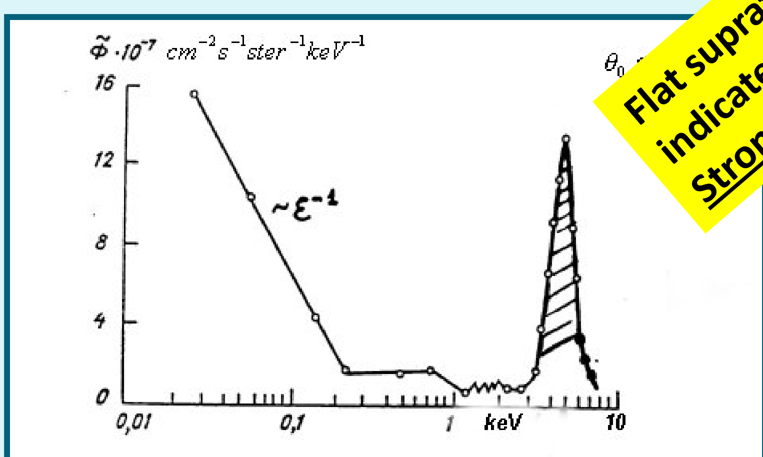

Beam of field-aligned electrons over the II class arc [Arnoldy et al., 1974]

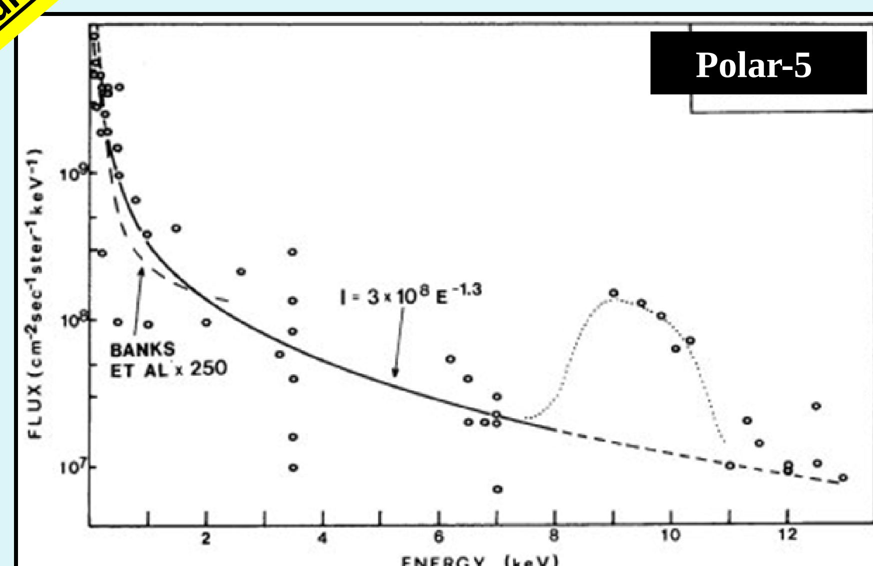

Flat suprathermal spectra indicate electron acceleration by Strong Langmuir Turbulence

Beam-Plasma Instability

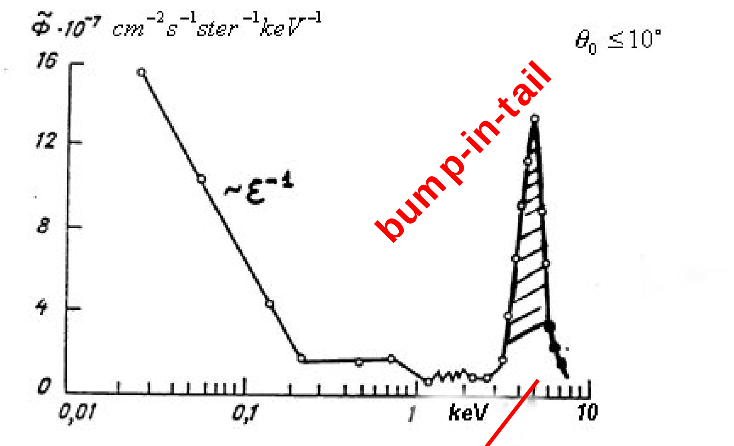

Beam of field-aligned electrons over the II class arc
[Arnoldy et al., 1974]

Inverse Landau damping

$$\Gamma_b \sim \omega_p \frac{\pi n_b}{n_e}\left(\frac{\varepsilon_b}{\Delta\varepsilon_{\parallel}}\right)^2 - \nu_e(T_e)$$

EISCAT UHF ISR

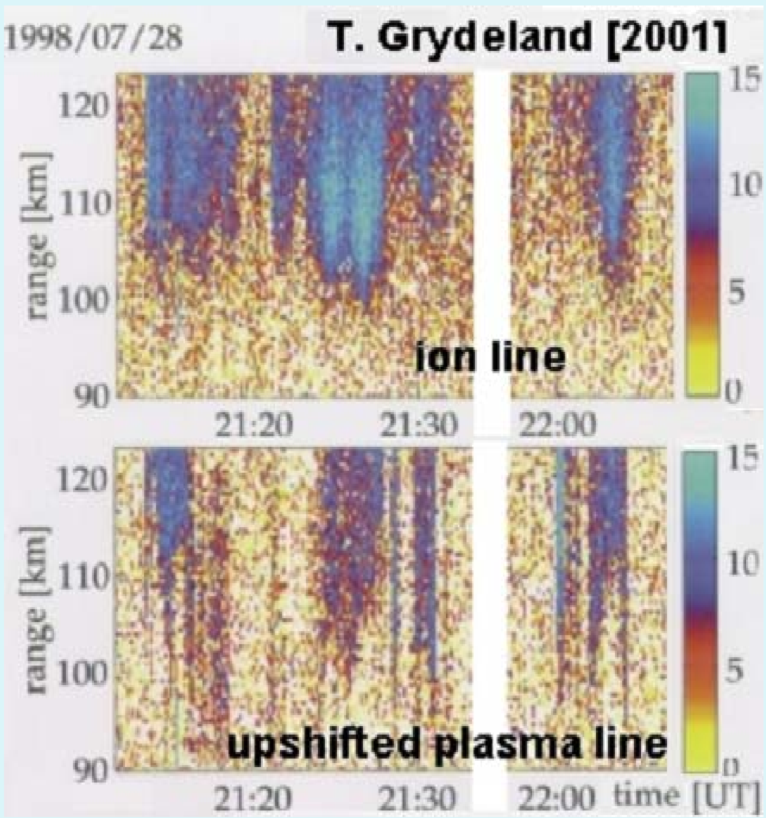

Langmuir waves grow at altitudes > ~110 km

Strong LT in auroral plasma

Flat accelerated electron spectrum

$$n_b^{(th)} \approx 10^{-6}\left(1+\frac{2\nu_e\,\varepsilon_b}{3\omega_p\,T_e}\right)n_e \quad \rightarrow \quad \text{SLT} \quad \rightarrow \quad F_a(\varepsilon_\parallel)\simeq\frac{2p_a-1}{v_{\min}}n_a\left(\frac{\varepsilon_{\min}}{\varepsilon_\parallel}\right)^{p_a}$$

$(p_a \simeq 0.8\text{-}1)$

Joining condition

$$F_a(\varepsilon_{\min}) = F_0(\varepsilon_{\min})$$

➢ **Acceleration of *secondary* electrons**

$$\varepsilon_{min} \simeq 30(W_L/n_s T_e)^{-2/5}[\text{eV}]$$

n_s is the density of secondary electrons

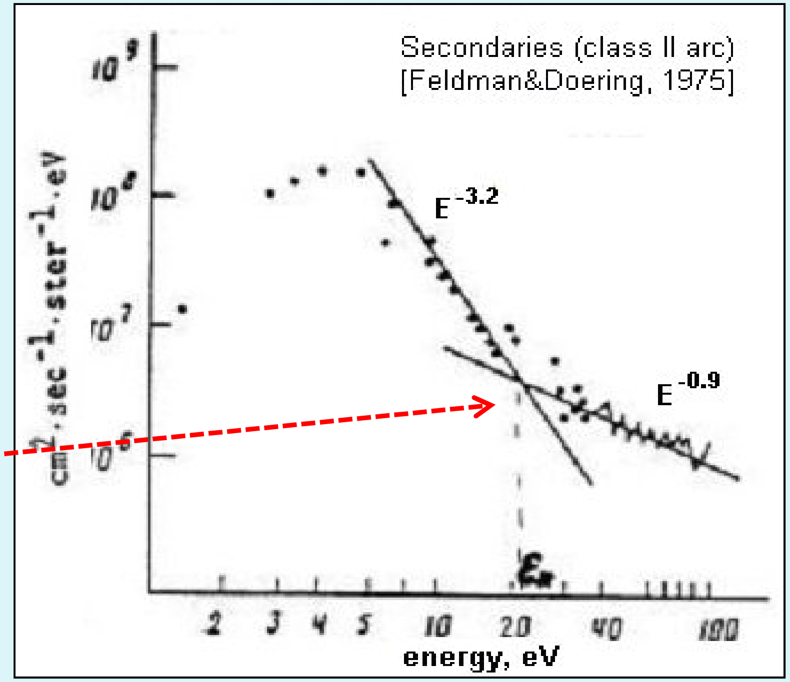

Mishin & Telegin, 1986

SLT Aurora

Mishin +, 1978-1989

➢ Effects of collisions on SLT

$$\Gamma_b \gg \nu_e > \frac{m}{M}\omega_p$$

As the collapse rate is smaller than Γ_b, the beam can excite waves *but* the trapped waves are damped faster than collapsing. As nonlinear transfer is reduced, the Langmuir wave energy grow until collapse will be possible.

the limiting collision frequency

$$\nu_* = \omega_p \left(\frac{m}{M}\,\frac{\Gamma_b}{\omega_p}\right)^{1/2}$$

Wave energy density

$$W_L/n_e T_e \simeq \frac{3M}{m}\left(\frac{\nu_e}{\omega_p}\right)^2$$

Ionization by accelerated electrons

$$T_e \approx \sqrt{3\varepsilon_{ion}\frac{W_L}{n_e}}$$

$$q_{ion}^{(t)} \simeq 10\ \nu_e(T_e)\ n_b\ \frac{T_e}{\varepsilon_{ion}}\left(\frac{\varepsilon_b}{\Delta\varepsilon_{\|}}\right)^2$$

Plasma Turbulence Layer

Schematic of altitude-profiles

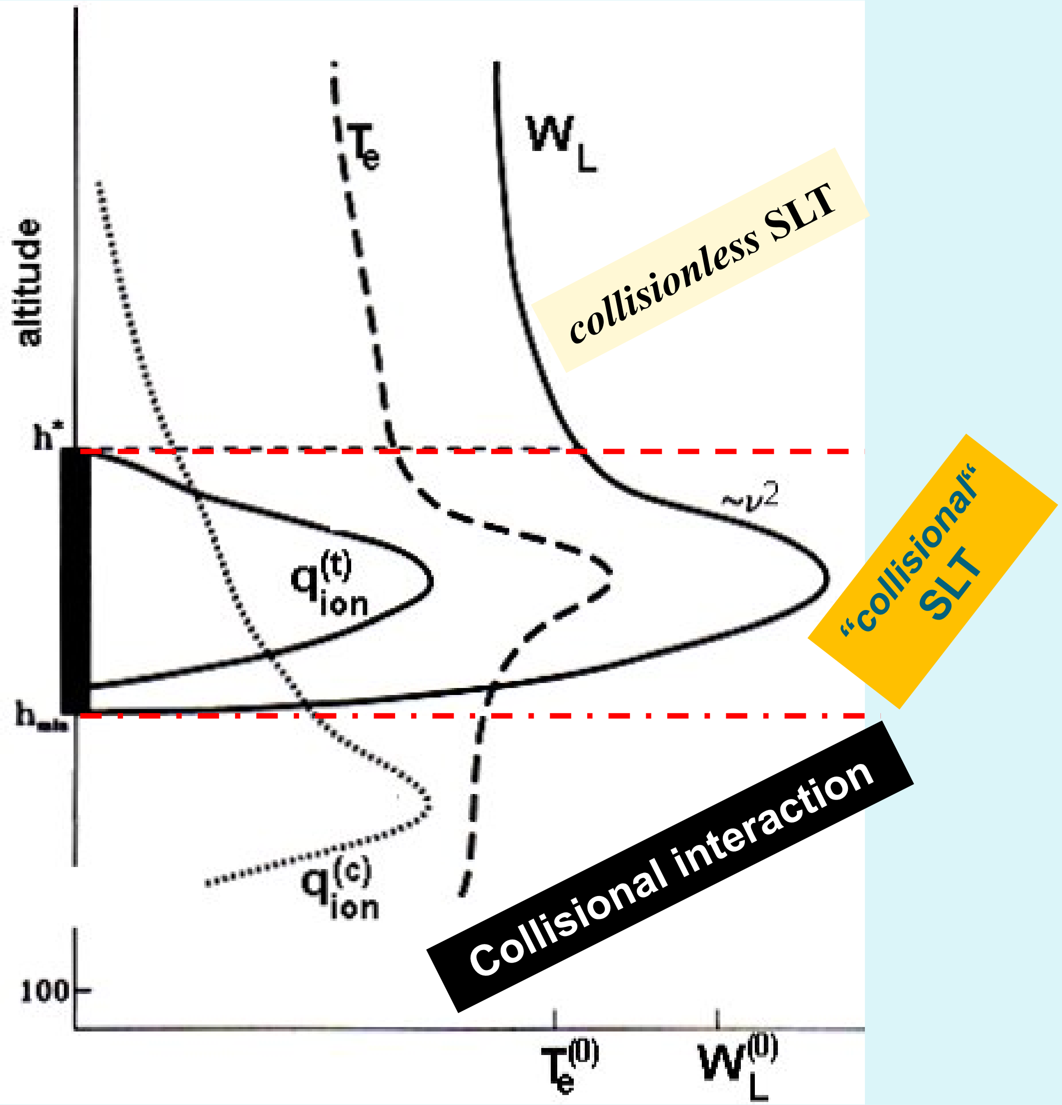

EISCAT UHF ISR

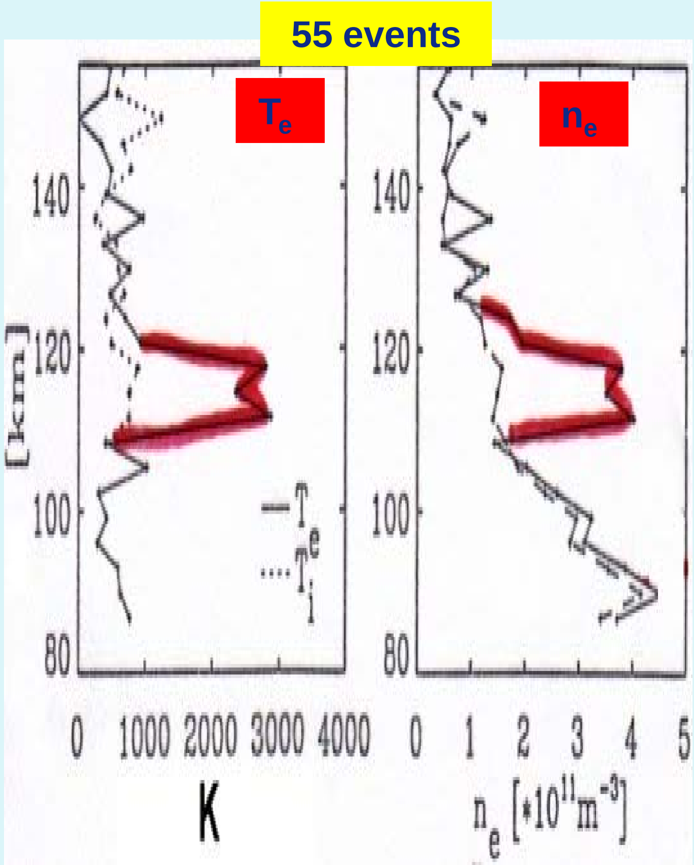

High Frequency Active Auroral Research Program

HAARP Research Station, Gakona (62.4 N, 145 W)

http://haarp.alaska.edu

- 180-element phased HF antenna array
- 3.6 MW radiated power → 1.3 GW *ERP*
- beam pointing +/-30 deg off vertical

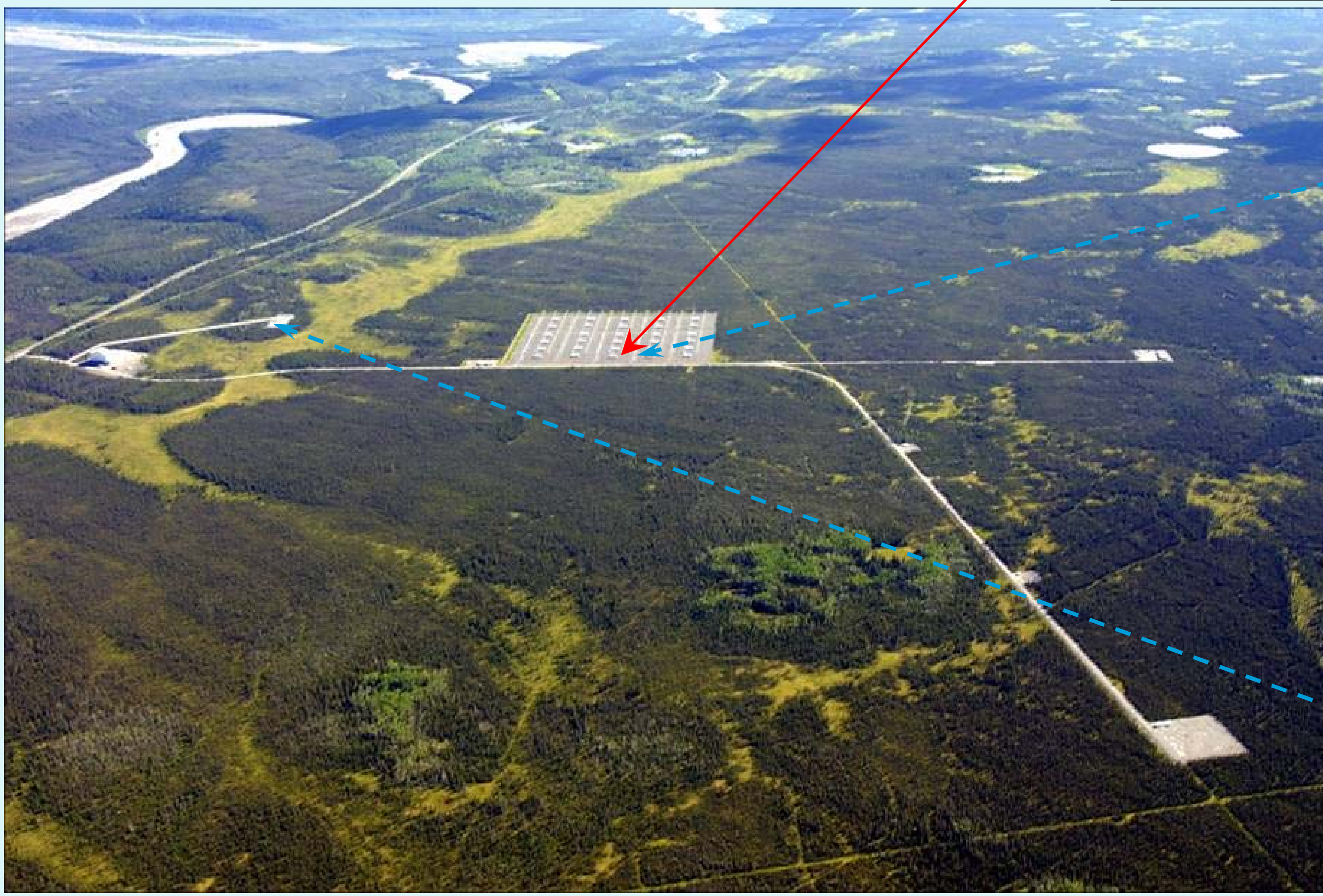

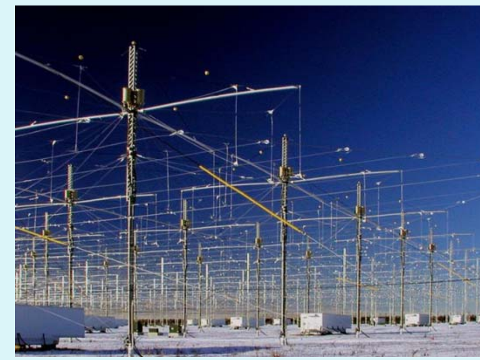

frequency : 446 MHz peak power : 512 kW
aperture : 219.8 m^2 (16 panels)
beam width : 4° (north-south), 2.5° (east-west)

HAARP Optical Diagnostics

- 2 optical shelters
- 6” telescope up and running in open-air 14’ dome; utilizing same CCD cameras
- Imager and photometer mounted on hydraulic lift and motorized stage under 5’ clear dome
- Photometer electronics upgraded: 3 channels with one filter wheel
- 3.5” Optical imager (bare CCD)
- 4-channel all-sky low-light webcam operates year-round (except June)

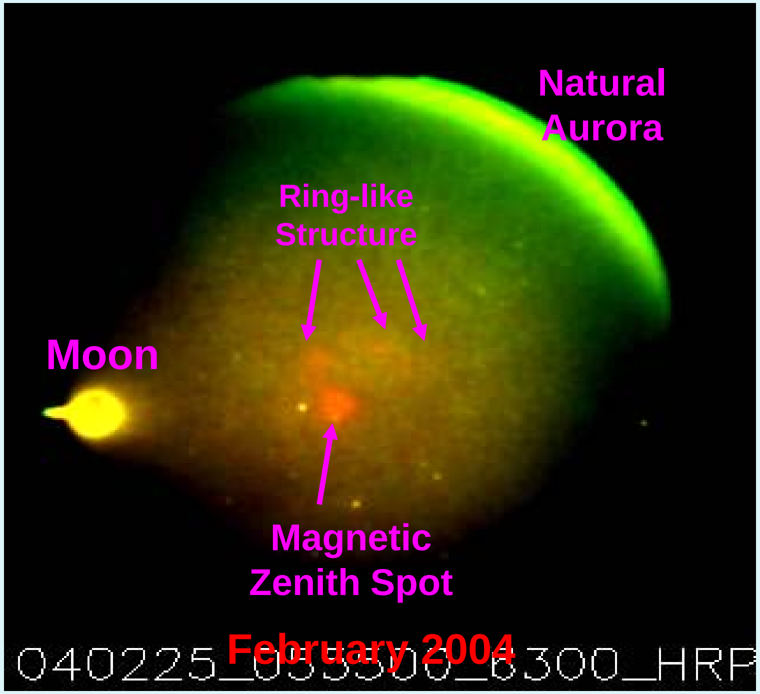

Pedersen et al., 2008

Dependence on HF-beam Pointing Angle

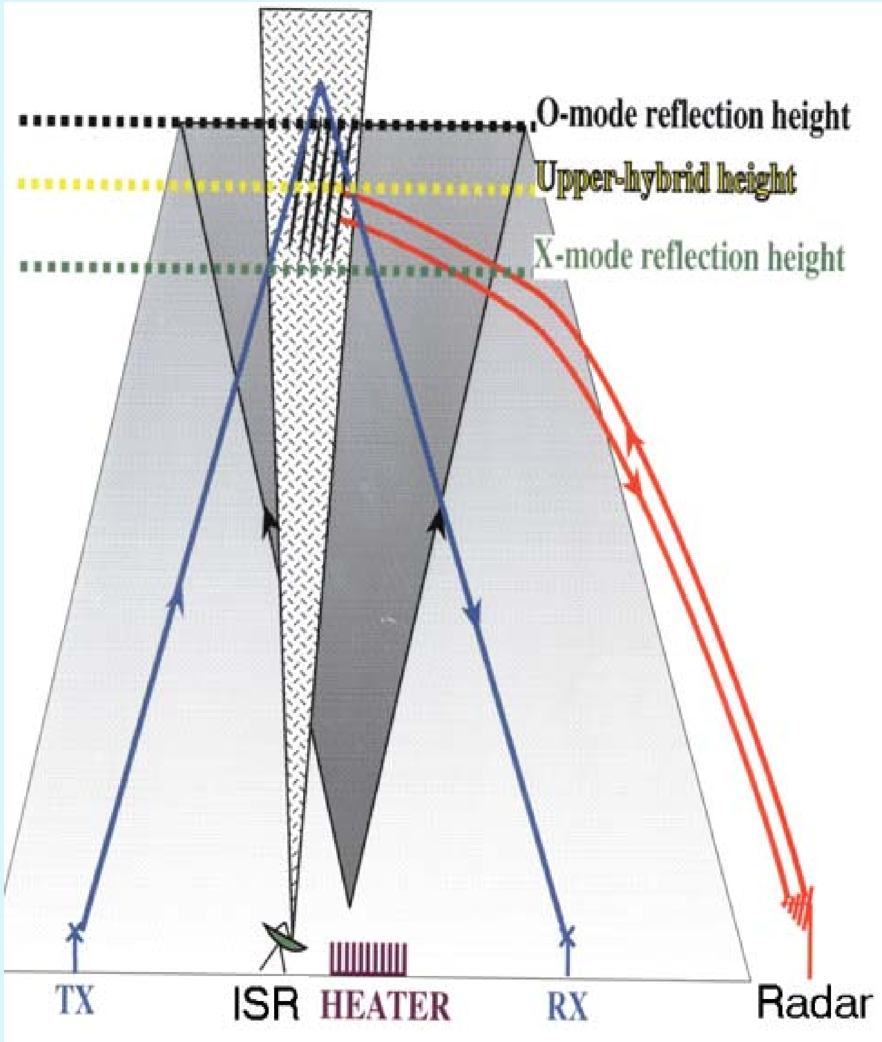

Ray trajectories, f_0>5.5 MHz

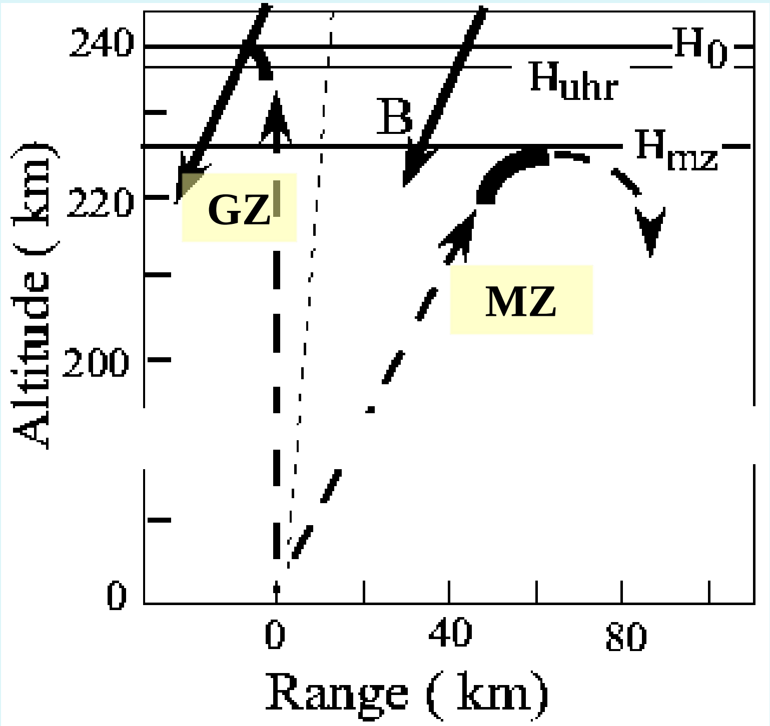

$f_P(H_0) = f_0$

$f_{UH}(H_{uhr}) = f_0$

$f_P(H_{mz}) = f_0 \cos\chi$

Accelerated Electrons

- Tromsø: 5.423 MHz, 375 MW, MZ, 4/2-min on/off.
- Te enhancements 3000-3500 K

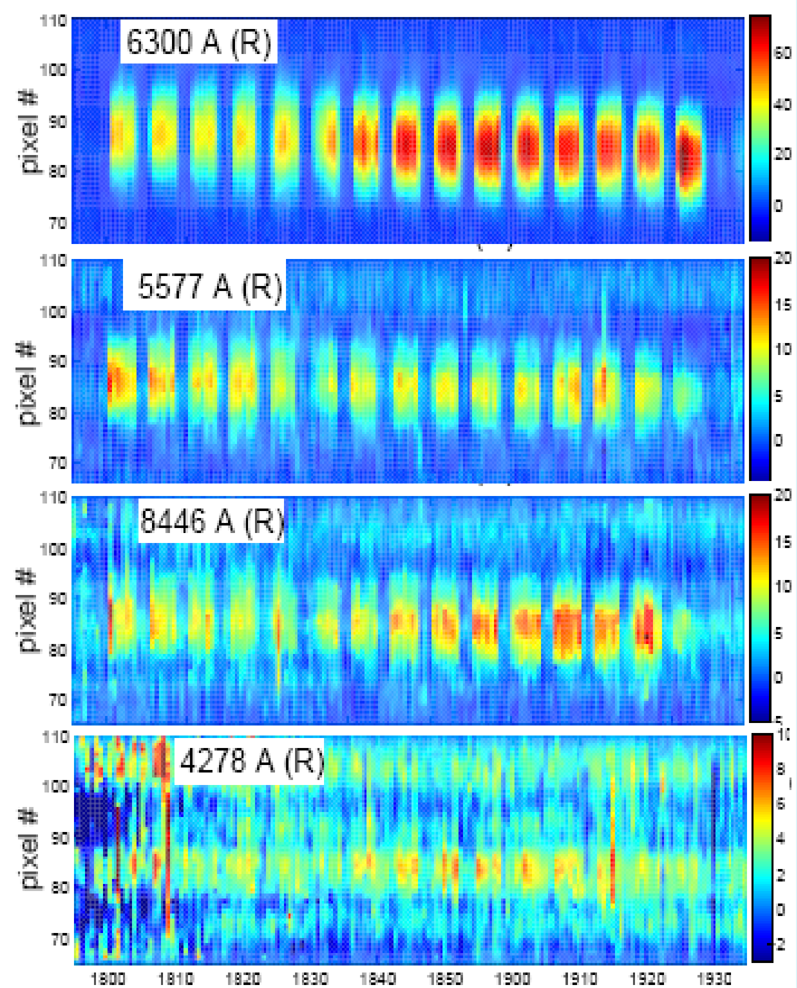

Keograms of the ALIS observations after background subtraction

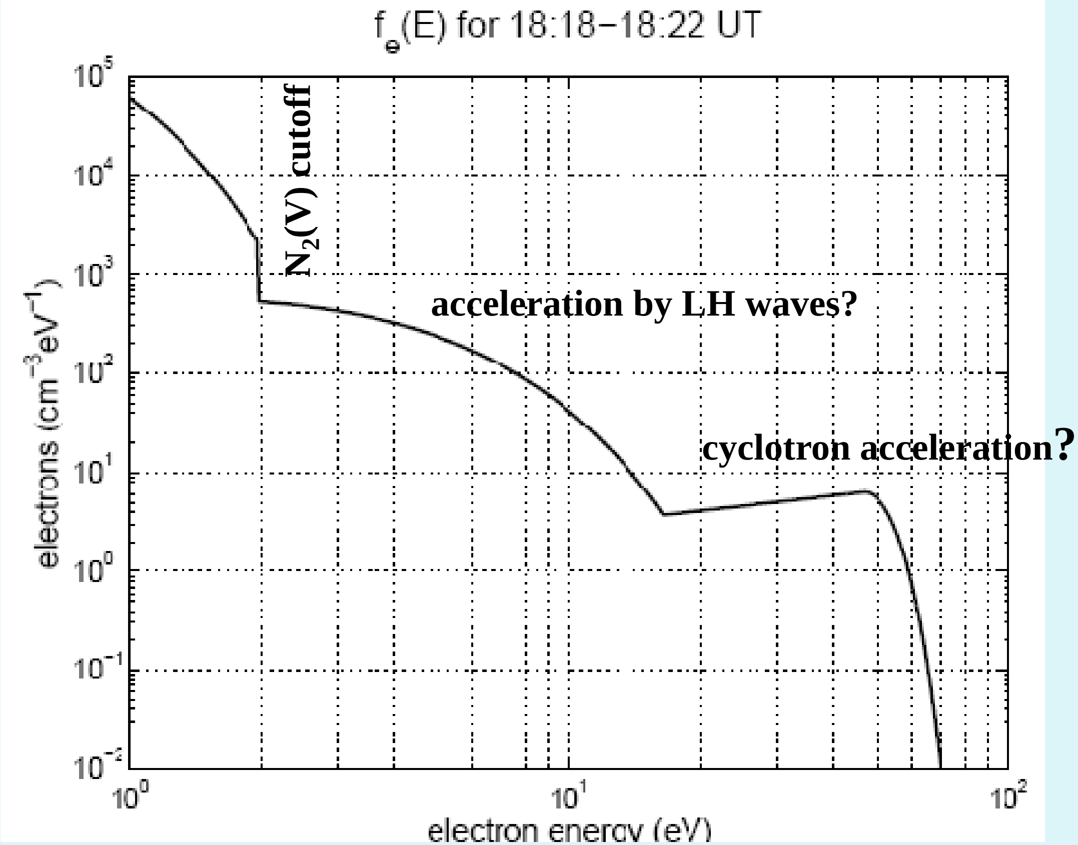

Gustavson et al., 2007

Parametric Decay Instability

$$EM_0 \rightarrow EP_1 + EP_2$$

- Electromagnetic Pump Wave EM_o
- Daughter HF (EP_1) and LF (EP_2) waves

✓ EP_1 = L*angmuir* ***and*** U*pper*H*ybrid*/E*lectron*B*ernstein*

✓ EP_2 = I*on*A*coustic* ***and*** L*ower*H*ybrid*

➢ Matching Conditions

- $k_o = k_1 + k_2$
- $\omega_o = \omega_1 + \omega_2$

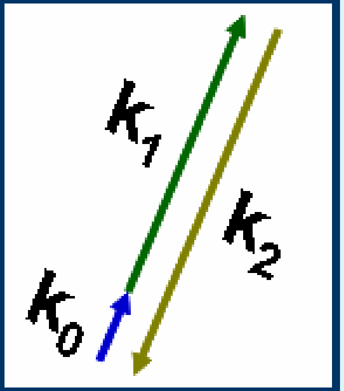

Thermal Parametric Instability

Conversion of the pump wave on field-aligned density irregularities

$$O + \delta n_{FAI} \rightarrow UH$$

For $\Delta n \rightarrow 0$ and $\left|\rho_{uh}^2 \frac{d^2}{dx^2}\right| \ll |\epsilon_{\perp 0}|$

near H_{UHR}

$$\delta E_{uh} \simeq \frac{p \cdot E_0}{\epsilon_{\perp 0}} \cdot \frac{\Delta n(x)}{n_0}$$

Here $\rho_{uh} = r_D \sqrt{\frac{3}{1-(2\Omega_c/\omega_o)^2}}$

$\epsilon_{\perp 0} = 1 - \omega_p^2 / \left(\omega_0^2 - \Omega_c^2\right) \lesssim 0$ above/below H_{uhr}

$\epsilon_{\perp 0} < 0$ above H_{uhr} and hence $\delta E_{uh} > 0$ if $\Delta n < 0$ → excess heating in density rarefactions *and* deficit heating in compressions.

Positive feedback:
UH-trapping *inside striations* → enhanced heating → further depletion

The growth time for the TPI is of order seconds

Airglow at MZ in an *underdense* ionosphere

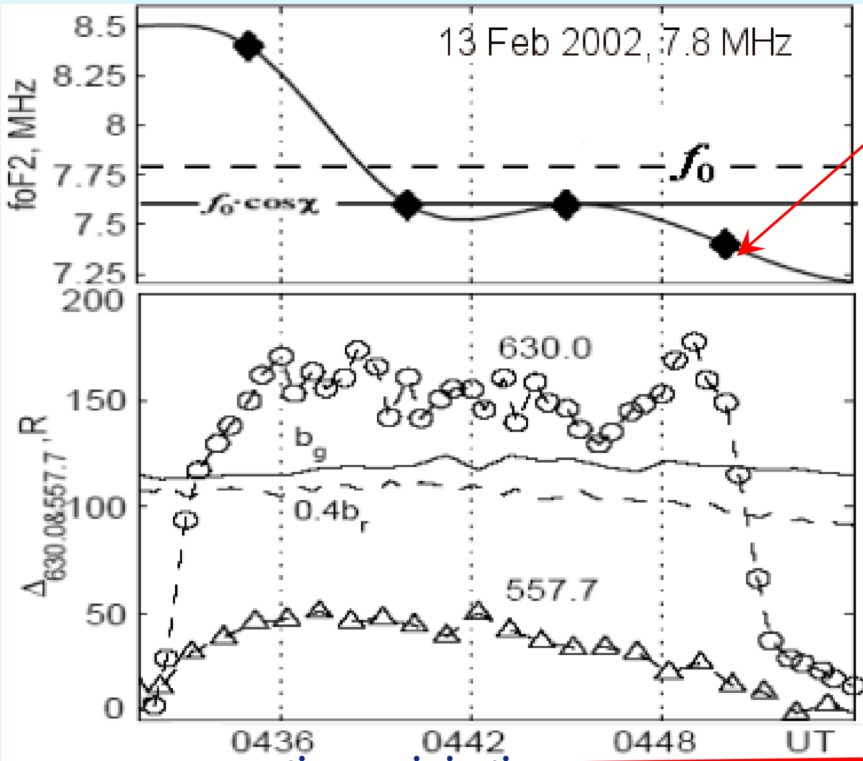

continuous injection

Fig. 6. Summary plot of the variation of the HF-induced airglow at MZ with $foF2 - f_0$. Here 7.8, ...4.5 stand for f_0=7.8, ...4.5 MHz;

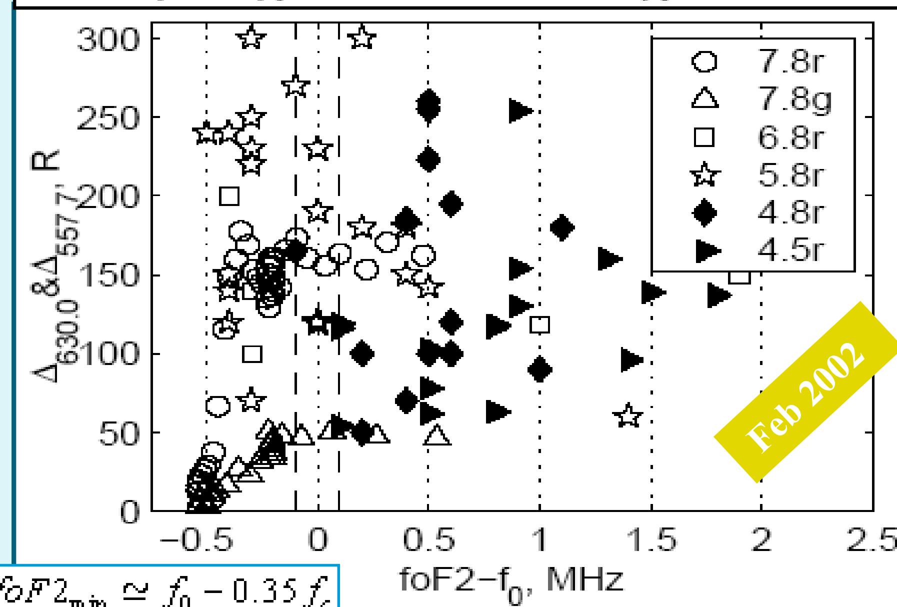

$foF2_{min} \simeq f_0 - 0.35 f_c$

O→ UH + LH

$$x^*_{uh}(H, f_0) \simeq \frac{2}{3} \frac{s(s^2-4)}{s^2-1} \frac{f_0 - f_{uhr}(H)}{f_c(H)}$$

Mishin et al., 2005

Underdense F-region

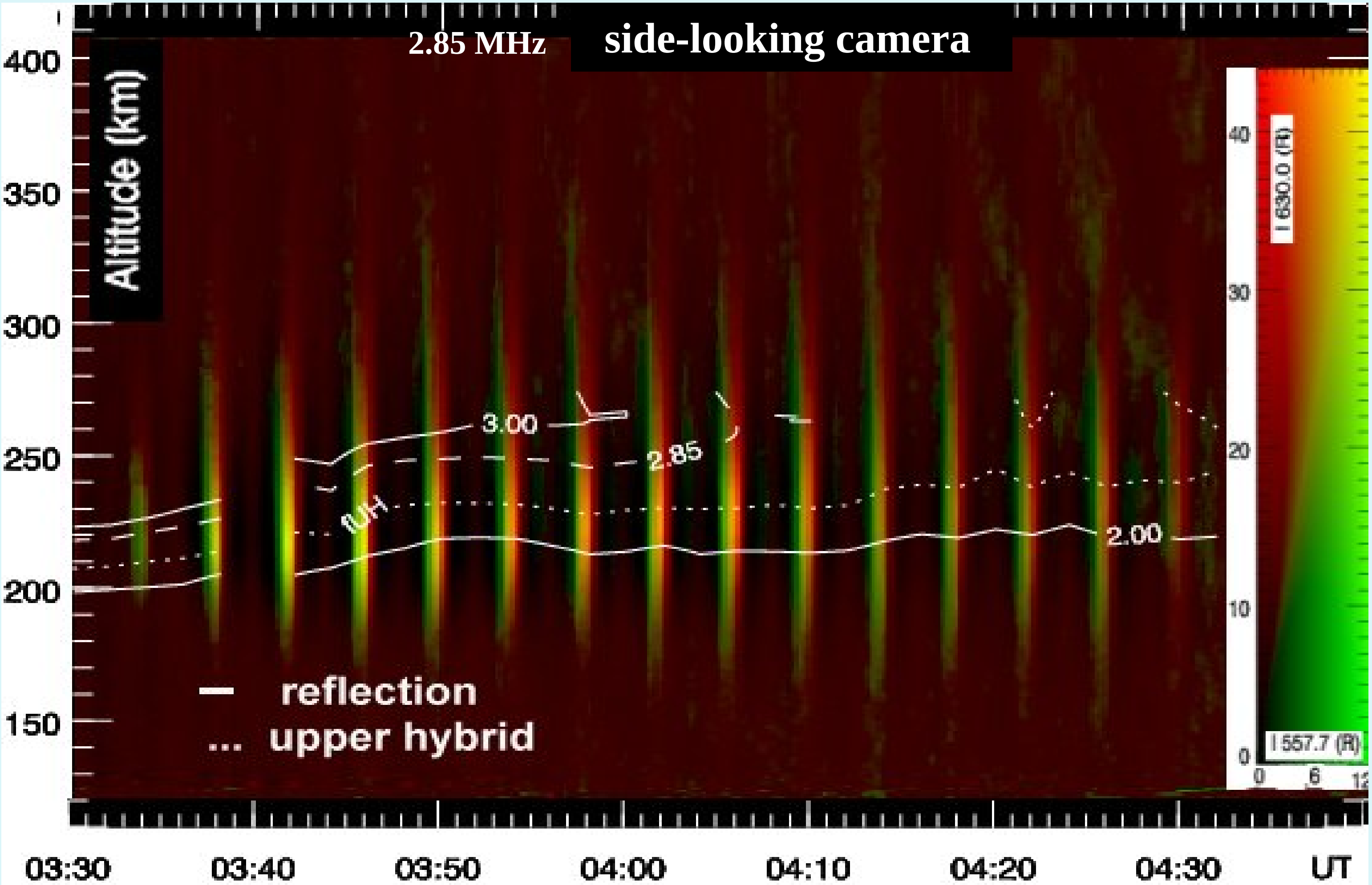

Pedersen et al., 2008

Second electron gyroharmonic

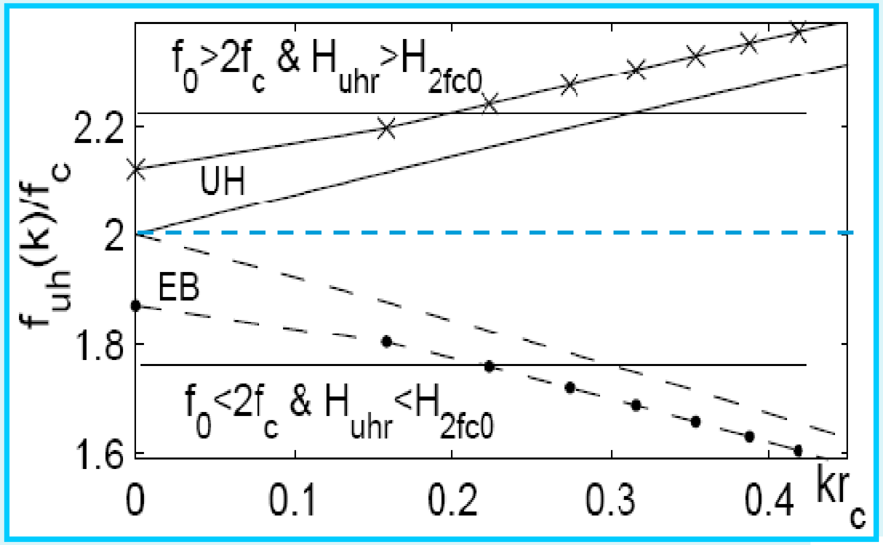

O-mode reflection at and above H_{2fc0} →
TPI & PDI_{EB} above & below H_{2fc0}

Suppression of PDI_L by striations

O-mode reflection below H_{2fc0} →
PDI_{EB} & PDI_L

The TPI_{UH} threshold near the second GH strongly depends on the frequency mismatch $\delta_{UHR} = \frac{f_{UHR} - 2f_C}{2f_C}$

The TPI threshold

$$\frac{E_o^2}{4\pi n T_e} > \frac{3\nu_e}{\omega_o}\left(\lambda_\parallel^2 l_e^2 + \lambda_\perp^2 r_c^2\right)\frac{\partial(\omega^2\epsilon_\perp(\omega))}{\partial\omega^2}$$

Grach, 1979

$\approx 16/3$ for $|\delta_{UHR}| < \frac{3}{4}\kappa_\perp r_C$

>20, otherwise

$$\delta_{UHR} < \delta_{UHR}^{(m)} \simeq 0.01$$

2GH, 25-Feb-2004 (2.5/2.5 min on/off, 10 MW at MZ)

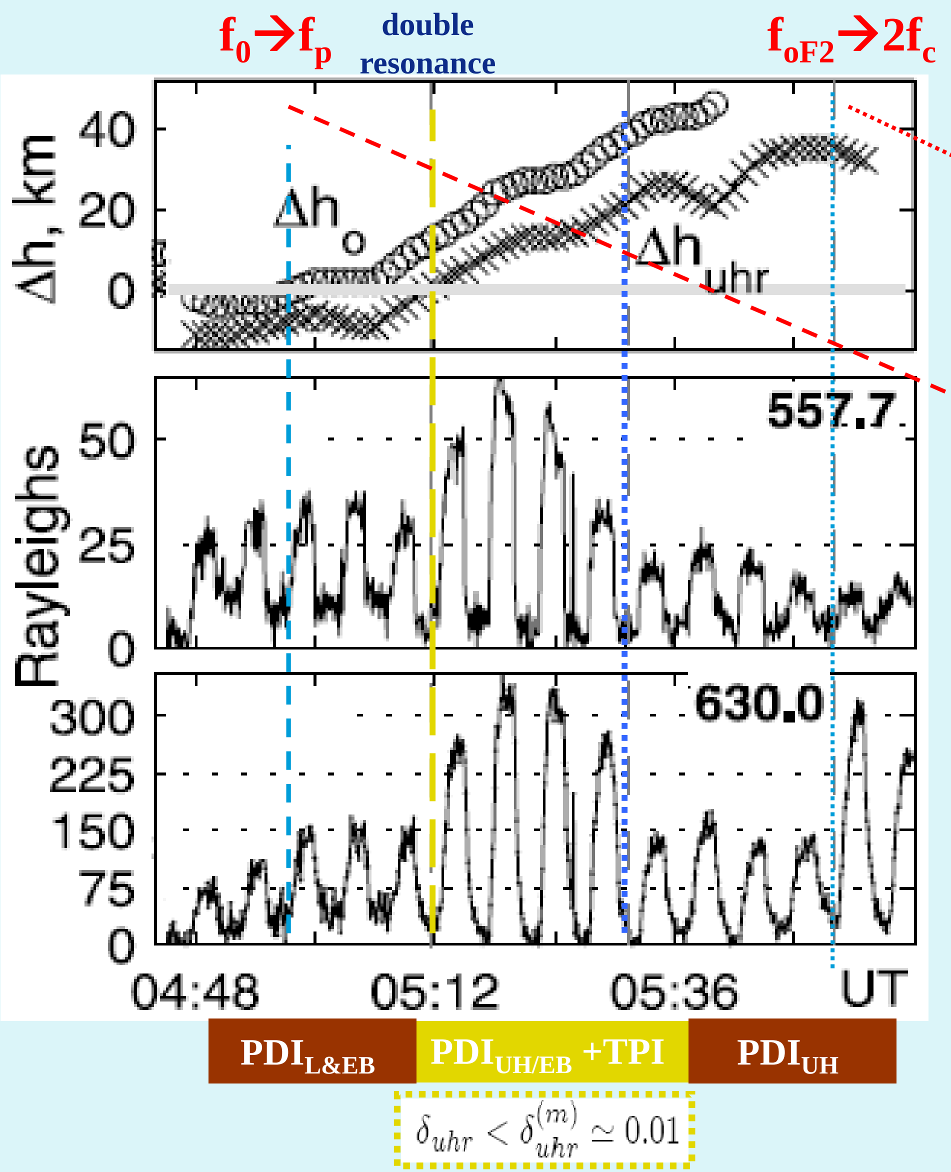

Height profiles of f_P

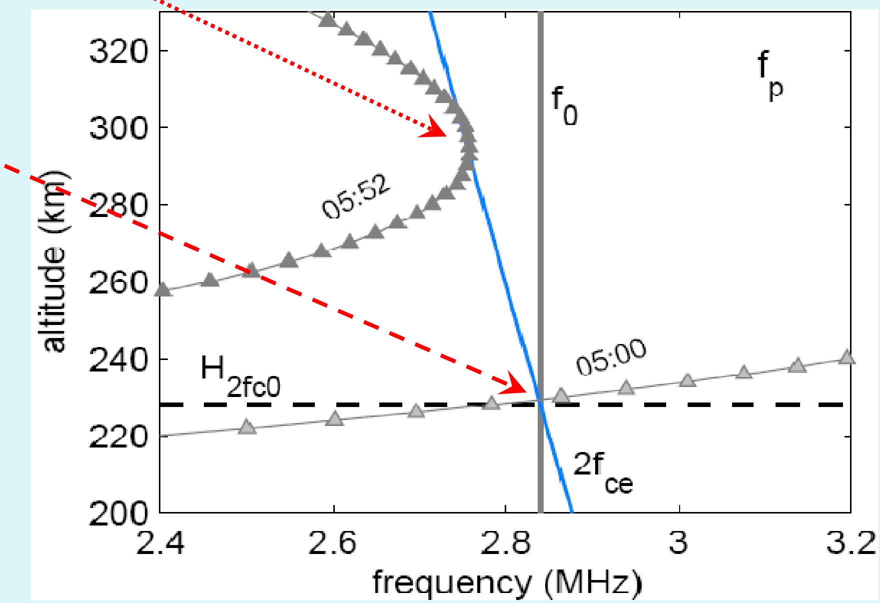

- Green/Red ratio > 0.1
- No change when foF2 <f_0

Mishin et al., 2005

2GH, 4-Feb-2005 (10 MW, 1/2 min on/off)

$f_0=f_p$

double resonance

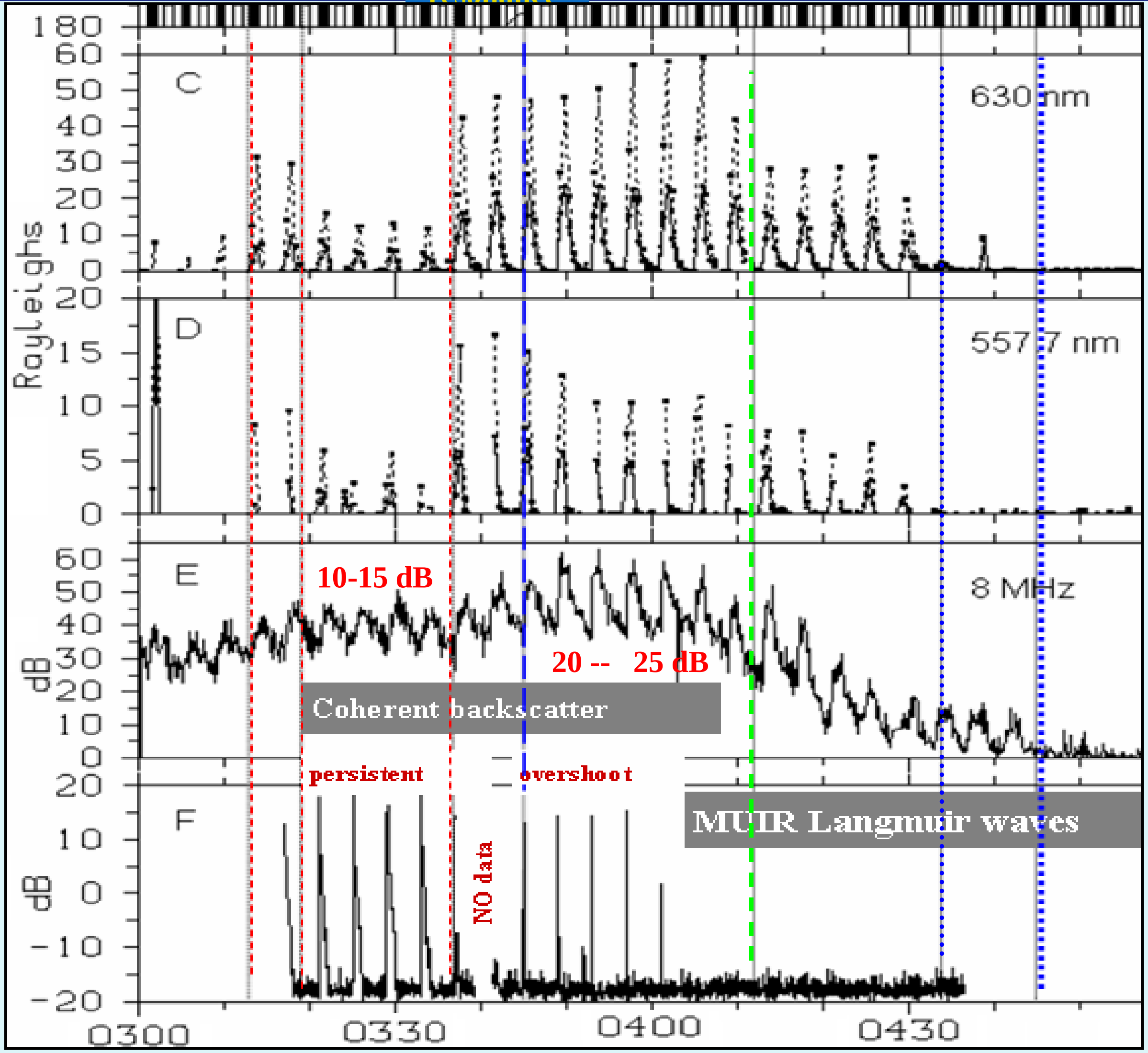

Kosch et al., 2007

$PDI_{L\&EB}$

$PDI_{EB\&UH}$ +TPI

PDI_{UH}

Summary

- Common characteristics of natural and man-made auroras are flat suprathermal spectra and altitude profiles consisting of two narrow peaks displaced by ~10 km.
- These features can be explained by accounting for strong Langmuir turbulence excited by precipitating/injected electron beams in weakly-collisional ionospheric plasma.
- Up to three parametric instabilities (PDI_L, $PDI_{UH/EB}$, and TPI) act simultaneously during HF heating at the magnetic zenith.
- Optical and radar observations during a frequency pass through the second GH show the coexistence of PDI_L and $PDI_{UH/EB}$ below 2GH and of the parametric decay and thermal parametric instabilities just above 2GH.
- Airglow at MZ persists after the critical F-layer frequency drops below the pump frequency by ~0.5 MHz, in agreement with the development of the PDI_{UH} .